Chen *et al. Molecular Cancer* (2024) 23:196
https://doi.org/10.1186/s12943-024-02108-6

Molecular Cancer

RESEARCH Open Access

Discovery of vitexin as a novel VDR agonist that mitigates the transition from chronic intestinal inflammation to colorectal cancer

Yonger Chen[1,2†], Jian Liang[2†], Shuxian Chen[3†], Nan Lin[3], Shuoxi Xu[2], Jindian Miao[2], Jing Zhang[2], Chen Chen[2], Xin Yuan[4], Zhuoya Xie[5], Enlin Zhu[6], Mingsheng Cai[1*], Xiaoli Wei[5*], Shaozhen Hou[2*] and Hailin Tang[5*]

Abstract

Colitis-associated colorectal cancer (CAC) frequently develops in patients with inflammatory bowel disease (IBD) who have been exposed to a prolonged state of chronic inflammation. The investigation of pharmacological agents and their mechanisms to prevent precancerous lesions and inhibit their progression remains a significant focus and challenge in CAC research. Previous studies have demonstrated that vitexin effectively mitigates CAC, however, its precise mechanism of action warrants further exploration. This study reveals that the absence of the Vitamin D receptor (VDR) accelerates the progression from chronic colitis to colorectal cancer. Our findings indicate that vitexin can specifically target the VDR protein, facilitating its translocation into the cell nucleus to exert transcriptional activity. Additionally, through a co-culture model of macrophages and cancer cells, we observed that vitexin promotes the polarization of macrophages towards the M1 phenotype, a process that is dependent on VDR. Furthermore, ChIP-seq analysis revealed that vitexin regulates the transcriptional activation of phenazine biosynthesis-like domain protein (PBLD) via VDR. ChIP assays and dual luciferase reporter assays were employed to identify the functional PBLD regulatory region, confirming that the VDR/PBLD pathway is critical for vitexin-mediated regulation of macrophage polarization. Finally, in a mouse model with myeloid VDR gene knockout, we found that the protective effects of vitexin were abolished in mid-stage CAC. In summary, our study establishes that vitexin targets VDR and modulates macrophage polarization through the VDR/PBLD pathway, thereby alleviating the transition from chronic colitis to colorectal cancer.

†Yonger Chen, Jian Liang and Shuxian Chen contributed equally to this work.

*Correspondence:
Mingsheng Cai
caimingsheng@gzhmu.edu.cn
Xiaoli Wei
weixl@sysucc.org.cn
Shaozhen Hou
hsz0214@gzucm.edu.cn
Hailin Tang
tanghl@sysucc.org.cn

Full list of author information is available at the end of the article

Highlights

- Deficiency in VDR accelerates the progression from chronic colitis to colorectal cancer.
- Vitexin regulates transcription by targeting VDR and upregulating its nuclear expression.
- Vitexin induces M1 polarization of macrophages in the tumor microenvironment via the VDR/PBLD signaling pathway, mitigating the progression from chronic colitis to colorectal cancer in mice.

Keywords Vitexin, Macrophage, Vitamin D receptor, Colitis-associated colorectal cancer

Introduction

Colorectal cancer (CRC) is one of the leading causes of cancer-related mortality globally, with over 20% of cases linked to chronic inflammation [1]. Colitis-associated colorectal cancer (CAC) represents a particularly aggressive subtype of CRC that occurs in patients with inflammatory bowel disease (IBD) who have been in a chronic inflammatory environment for a long time [2, 3]. The largest cohort study in China showed that homologous recombination pathway gene mutations are another major genetic risk factor for heterogeneous clinical phenotypes of colorectal cancer [4]. Unlike sporadic CRC, which typically progresses through the adenoma-dysplasia-carcinoma sequence, CAC is characterized by the accumulation of somatic mutations that facilitate the progress transition from inflammatory mucosa to dysplasia to carcinoma [5], and patients with CAC are often diagnosed at an advanced stage and with a poor prognosis [6]. Thus far, the management of colorectal cancer has encountered substantial challenges, particularly due to the development of drug resistance in treatments targeting the disease [7–10]. Studies have shown that mitochondria in colorectal cancer stem cells are a target for drug resistance [11]. Inflammatory damage accelerates the onset and progression of CAC [12]. This inflammatory signaling is mediated through dynamic crosstalk between cancer cells and tumor microenvironment (TME) cells. Therefore, exploring the intrinsic connection between cancer cells and TME cells is also crucial for a better understanding of carcinogenesis.

The TME consists of various types of non-malignant stromal cells, including macrophages, neutrophils, lymphocytes, endothelial cells, and cancer-associated fibroblasts (CAFs). Tumor-associated macrophages (TAMs) play a pivotal role in tumor progression, metastasis, and recurrence following treatment [13, 14]. The plasticity and heterogeneity of macrophages allow them to be classified along the M1-M2 polarization axis [15–17]. Tumor-associated macrophages usually exhibit an M2-like phenotype with pro-tumor functions, whereas M1 macrophages have anti-tumor functions. Consequently, reprogramming TAMs to adopt an M1-like phenotype represents a promising strategy to promote tumor regression [18, 19]. Various approaches exist for selecting the M1 phenotype from TAMs or reprogramming TAMs from an M2 to an M1 phenotype, including TLR agonists, monoclonal antibodies targeting M1 phenotype suppressor proteins, and other compounds [20]. Targeted therapy usies utilizing small molecule compounds can specifically target genes in tumor cells, precisely acting on cancer cells to inhibit proliferation and reduce damage to normal cells, providing new insights for cancer treatment. Numerous studies have demonstrated that small molecule monomers derived from traditional Chinese medicine can exert therapeutic effects by targeting specific proteins. Vitexin, a flavonoid compound, has been reported to possess protective effects on the intestines. Our previous research indicated that vitexin significantly modulated macrophage polarization in the intestines of azoxymethane (AOM)/ dextran sodium sulfate (DSS) mice and exhibited protective effects on the intestines [21]. Despite significant advancements in our understanding of tumorigenesis, the complexities underlying the interactions between cancer cells and macrophages following vitexin exposure, particularly within the immune microenvironment, remain inadequately elucidated. The role of vitamin D receptors (VDR) in the pathogenesis of colorectal cancer and colitis has been well established. Notably, patients suffering from both inflammatory bowel disease and colorectal cancer often exhibit vitamin D/VDR deficiencies. Early downregulation of VDR has been observed in the onset of colitis, correlating with the development of larger and more numerous tumors in VDR-deficient models of CAC [22, 23]. Recent investigations have indicated that vitamin D activity becomes dysregulated in advanced cancer stages, although it is known to modulate the interactions between immune and cancer cells, thereby inhibiting the production of pro-inflammatory cytokines [24]. Despite extensive research on vitamin D, critical questions regarding the biological role of intestinal VDR during the transition from colitis to CAC remain unresolved. Therefore, it is important to search for novel VDR agonists and thus explore their therapeutic role and mechanisms in inflammatory cancers. Similarly, the changes occurring in macrophages during the transition from inflammatory bowel disease to CAC are complex. Within the tumor microenvironment, both VDR and macrophages are implicated in the progression of CAC, but whether they are closely linked or functionally independent remains unclear. Considering the multiple functional roles of the

VDR in the development of CAC, the cellular and molecular mechanisms by which the VDR regulates macrophages and thereby protects the host are important.

In this study, we established a mouse model of chronic colitis progressing to colorectal cancer (mid-term CAC) and demonstrated that myeloid-specific VDR knockout mice exhibit low VDR expression in the colon, which negatively correlates with the presence of M2-type macrophages. We confirmed that vitexin can target VDR and promote its transcriptional functions. We used a co-culture of macrophages and cancer cells to simulate the vitexin regulation of macrophages in the tumor microenvironment in a VDR-dependent manner and found that this regulation is achieved through the VDR/phenazine biosynthesis-like domain-containing protein (PBLD) pathway. In addition, we used a mouse model with myeloid-specific VDR knockout to study the protective effect of vitexin on VDR during inflammation and tumorigenesis. Our findings elucidate novel pathways and candidate therapeutic agents for addressing the transformation of chronic intestinal inflammation into colorectal cancer by regulating the polarization of macrophages in the tumor microenvironment.

Materials and methods

Materials

Vitexin (HPLC purity > 98%), and Calcitriol were purchased from Sigma-Aldrich. AOM were purchased from Sigma Aldrich. DSS were purchased from MP Biomedicals. Pronase were purchased from Roche. For in vitro experiments, vitexin was dissolved in DMSO and Calcitriol in water, and for in vivo studies, vitexin was dissolved in 1% carboxymethylcellulose sodium (CMC-Na) solution and Calcitriol in saline. Recombinant human protein VDR was constructed at KMD Bioscience (Tianjin, China) and recombinant human protein VDR-LBD was constructed and sequenced at DetaiBio. (Nanjing, China). APC anti-Mouse F4/80 Antibody and FITC anti-Human/Mouse CD11b Antibody were purchased from MULTI SCIENCES. PE/Cyanine7 anti-mouse CD206 (MMR) Antibody, PE anti-Nos2 (iNOS) Antibody, PE/Cyanine7 anti-human CD206 (MMR) Antibody and PE anti-human CD86 Antibody were purchased from BioLegend. PcDNA3.1(+)-VDR-3×FLAG, pGL4.10-CYP24A1 promoter, Wide-Type, pCMV3-flag-ratVDR, pCMV3-flag-ratVDR- T287A were constructed and sequenced by OBio. (Shanghai, China). Extraction kits for cell membrane and nucleus fractions were performed by beyotime (Shanghai, China).

Animals

SPF-grade Lyz2-Cre (JAX 004781) was purchased from the Jackson Laboratory, $VDR^{fl/fl}$ was purchased from GemPharmatech (Jiangsu, China), and Lyz2Cre-$VDR^{fl/fl}$ ($VDR^{\Delta M\Phi}$) mice were generated by crossing $VDR^{fl/fl}$ (VDR^{flox}) mice with Lyz2-Cre (Figure S2, Supporting Information). The purchased $VDR^{Fl/wt}$ transgenic male mice will be co-housed with wild-type female C57BL/6J background mice at a ratio of 1:2 for mass breeding. After the newborn mice reach 2 weeks of age, they will be numbered and their tails will be clipped for genetic identification, with the identified PCR primers (Table S1, Supporting Information).

SPF-grade male C57BL/ 6 J mice (18–22 g) were purchased from Guangzhou University of Chinese Medicine Laboratory Animal Centre. All mice were crossed with C57BL/6 for at least 10 generations. The animals were housed in the SPF-grade laboratory animal room of the Guangzhou University of Chinese Medicine and were given normal feed and free drinking water every day, with a relative humidity of 55 ± 5%, an indoor temperature of 22 ± 2 ℃, and 12 h of light. The bedding was changed every other day. The animals were acclimatized to the laboratory for at least 2 weeks before the start of the study. All animal experiments were conducted and analyzed in a blinded randomization manner.

AOM-DSS induced mid-stage colorectal cancer model

Mice were injected intraperitoneally with 10 mg/kg AOM (A5486, Sigma), followed by two cycles of 1.5% DSS in the drinking water on days 8–15 and 22–29 (referenced to previously published [25] literature but adapted). Disease progression was monitored by body weight measurements and DAI examination, and dissection was determined on day 36. The methodology for the determination of DAI is described in detail in Supplementary Table 2. At the end of the experiment, mice were executed, colon harvested and colon weight and length measured. Tumor load was quantified post-mortem by macroscopic examination of the colon.

Cell culture

THP-1 (Human Acute Monocytic Leukemia Cells) and RAW 264.7 (Mouse Mononuclear Macrophages Cells), is the most commonly used inflammatory cell model. CT26.WT (Mouse Colorectal Carcinoma Cells) are undifferentiated cells induced by N-nitroso-N-methylurea (NNMU). HCT 116 (Human Colorectal Carcinoma Cells) was isolated from male patients with colon cancer. Human Embryonic Kidney Cells (HEK) 293T cells, used as tool cells for plasmid transfection. All cells were purchased from Procell (Wuhan, China). CT26.WT, HCT116 cells were cultured in RPMI-1640 medium, and RAW264.7, HEK293T were cultured in DMEM medium supplemented with 10% heat-inactivated fetal bovine serum (FBS) and 100 U/ml penicillin-streptomycin. THP-1 cells were cultured in RPMI-1640

supplemented with 10% heat-inactivated FBS and 100 U/ml penicillin-streptomycin, with the addition of 0.05 mM β-mercaptoethanol, and PMA activation (Sigma, USA) THP-1 cells were used as human macrophage studies.

PBLD siRNA

THP-1 cells were transfected with PBLD or control siRNA (Tsingke, China) using Lipofectamine® 6000 Transfection Reagent (Beyotime, China) in Opti-MEM I Reduced Serum Medium for 72 h. Then, the transfected cells were used for further research.

Cellular RNA sequencing

Total RNA was extracted from THP-1 cells using TRIzol (Accurate Biotechnology, China). Library sequencing was performed by Gene Denovo Biotechnology (Guangzhou, China) on an Illumina HiseqTM 2500/4000. Bioinformatics analysis was performed using Omicsmart, a real-time interactive online platform for data analysis (http://www.omicsmart.com).

PCR assay

Gene expression profiles were analyzed by macrophage differentiation PCR arrays (Wcgene Biotech, Shanghai, China) according to the manufacturer's protocol. β-actin and Gapdh were used as endogenous controls. Data were normalized to the reference gene based on cycle threshold (Ct) values. log2 (fold change) was calculated based on the $2^{-\Delta\Delta Ct}$ method.

Immunofluorescence staining and immunohistochemistry

The method according to a previous study [26]. Tissue wax blocks were hydrated by serial dewaxing, while cells were fixed by 4% paraformaldehyde. Then, after permeabilization with 0.05% Triton X-100 and sealing with 5% BSA, the cells were incubated with primary antibody at a dilution of 1:200 at 4 °C overnight. Fluorescently labeled secondary antibodies were used the following day. The stains were then counterstained with DAPI nuclear stain.

The operation of immunohistochemistry is carried out as described above. Following the procedures of primary antibody at a dilution of 1:200 at 4 °C overnight. After incubating with the secondary antibody the next day, DAI staining was performed. The sections were then stained with hematoxylin to visualize nuclei. The final processing steps included dehydration in graded alcohols, clearing in 100% xylene, and mounting. Images were taken with a fluorescence microscope equipped with a digital camera (Nikon, Tokyo, Japan).

Quantitative real-time PCR (qRT-PCR)

The method according to previous studies [27, 28]. Total RNA was isolated from cells using TRIzol (Accurate Biotechnology).The concentration of total RNA was determined using a Nanodrop 2000, and 1 μg of total RNA was converted to cDNA by reverse transcription according to the PrimeScript™ RT kit instructions in a CFX96 Touch The target gene was detected in a CFX96 Touch Real-Time RCR Detection System (Bio-Rad) detector using a SYBR Green PCR master mix kit with GAPDH as an internal reference, and the primer sequences of the target gene were designed by Shanghai Sangong Biotechnology Co. The primer sequences of target genes were designed by Shanghai Bioengineering Biotechnology Company. The relative expression of target genes was calculated by using the $2^{-\Delta\Delta}$Ct method for quantification, and the correlation analysis was carried out. Primer sequences are shown in Supplementary Table S3.

Western blot

The method is according to previous study [29]. In brief, proteins were isolated from cells and tissues and assayed by BCA assay. Proteins were separated by 8-12% gel electrophoresis separation kit (Beyotime, China) and transferred to polyvinylidene fluoride (PVDF) membranes using a semi-dry transfer apparatus (Bio-Rad). The membranes were blocked with 5% BSA for half an hour, and then the PVDF membranes were incubated with specific primary antibodies. The antibodies used in this study were as follows: VDR (Signalway Antibody, China, Cat#38397, 1:1000); PBLD (Proteintech, China, Cat#68317-1-Ig, 1:1000); PCNA (Affinity, China, Cat#AF0239, 1:1000); GAPDH (Affinity, China, Cat#AF7021, 1:3000); Histone (Affinity, China, Cat#BF9211, 1:3000). Immunoreactive bands were detected the following day with horseradish peroxidase-conjugated secondary antibodies and visualized by enhanced chemiluminescence. Analyses were performed using Image J analysis software and standardized against their respective controls.

Flow cytometry analysis

The method according to a previous study [30]. Cells were collected and resuspended in 500 μL of phosphate-buffered saline (PBS). Following a 30-minute incubation at room temperature with surface flow antibodies, the cells were centrifuged at 900 rpm for 4 min. The supernatant was discarded, and the cells were washed with PBS before being treated with a cell membrane-disrupting solution (Thermo Fisher, diluted 1:3) for 60 min. Afterward, the cells were washed again in PBS and incubated with polarization-associated flow antibodies for 1 h at room temperature. The cells were subsequently washed and resuspended in PBS containing 1% bovine serum albumin (BSA). Following another wash, the cells were resuspended in PBS with 1% BSA and analyzed using a NovoCyte Quanteon flow cytometer. Data were

processed using NovoExpress software, with specific labeling for F4/80, CD11b, iNOS (M1), and CD206 (M2) flow-through antibodies.

VDR binding assay

The binding of vitexin to VDR was determined by several methods

cellular thermal shift assay (CETSA), drug affinity responsive target stability (DARST), surface plasmon resonance assay (SPR), isothermal titration microcalorimetry assay (ITC), pull-down assay and immunofluorescence co-localization assay.

For CETSA, the CETSA method was performed according to the literature [31]. THP-1 cells were inoculated in a 100 mm dish and subsequently treated with FBS-free medium containing either 0.1% DMSO or 100 μM vitexin for 2 h the following day. Post-treatment, the cells were digested with trypsin, collected, and washed before being resuspended in 1 mL of PBS supplemented with a protease inhibitor. A 90 μL aliquot of this suspension was transferred into 0.2 mL PCR tubes and subjected to heating in a PCR machine for 3 min at temperatures ranging from 43 to 67 °C. 20 μL of RIPA buffer was added to each tube, and the precipitated proteins were removed by centrifugation at 15,000 × g for 20 min at 4 ℃ after thorough mixing. Subsequent supernatant manipulation was based on general Western blot experiments.

For DARTS, the DARTS method was performed according to the literature [32]. THP-1 cells were inoculated in a 100 mm dish at an appropriate density. The following day, the cells were harvested and lysed in 500 μL of RIPA buffer containing a protease inhibitor. The resulting lysate was aliquoted equally into 5 Ep tubes and subsequently diluted tenfold in TNC buffer (50 mM Tris-HCl, pH 8.0, 50 mM NaCl, 10 mM CaCl2). The samples were then incubated with 0.1% DMSO and varying concentrations of vitexin (0, 2.5, 5, and 20 μM) for 1 h at room temperature with gentle shaking. The samples were then proteolytically cleaved with protease (2.5 μg/mL) for 10 min. Subsequent operations were based on general Western blot experiments.

For SPR experiments, the interaction between vitexin and VDR (ligand-binding domain, LBD) protein was analyzed using a Biacore T200 system (GE Healthcare, Uppsala, Sweden). Recombinant VDR (LBD) at a concentration of 40 μg/mL was used to achieve non-covalent immobilization on the surface of the activated chip. The final level of immobilized VDR-LBD was approximately 12,000 reaction units (RU). Subsequently, different concentrations of vitexin (ranging from 6.25 μM ~ to 200 μM) were injected at a flow rate of 30 μL/min, and 1× PBST (1.37 M NaCl; 26.8 mM KCL; 81 mM Na_2HPO_4; 17.6 mM KH_2PO_4; Ph7.2-7.4, 0.05% Tween 20) was used as the running buffer. The results were analyzed using Biacore evaluation software (T200 version 1.0) and curves were fitted in 1:1 binding mode.

For the ITC experiments, the potential interaction between vitexin and VDR (LBD) was determined using the Nano-ITC instrument (TA instruments, USA) at 25 °C. A solution of 10 μM VDR (LBD) and 200 μM vitexin were dissolved in phosphate-buffered saline (PBS) containing 5% DMSO, and stirred at 250 rpm. Twenty titrations of 2.5 μL each were performed for each titration experiment. The heat of dilution of VDR protein was determined by titrating it into PBS. Data analysis was performed using the NanoAnalyze software package (TA Instruments). The total heat exchange during each injection of VDR into the vitexin solution was fitted to an independent model with variable parameters.

For pull-down experiments, Beaver-Beads streptavidin and biotinylated vitexin were utilized in this study. Specifically, 100 μL of biotinylated vitexin glycoside was added to 10 μL of streptavidin-agarose beads and incubated for 2 h at 25 °C. Controls included biotin, unbiotinylated vitexin, and untreated beads. The full-length prokaryotic proteins of the VDR were constructed at KMD Bioscience (Beijing, China), while the prokaryotic proteins corresponding to the VDR-LBD were constructed at Detai Bioscience (Nanjing, China). And mutant VDRs (T287) of the LBD structural domain was achieved by transfecting HEK-293 cells with the encoding plasmid under Lipofect 2000. Lysates were prepared from HEK-293 cells of the constructs and then the lysates were mixed into treated streptavidin-agarose beads. The mixture was incubated at 25 °C for 3 h with gentle shaking. The samples were then spun and washed three times. The samples were boiled with 5× loading buffer and loaded onto 10% polyacrylamide gels for western blot analysis.

For immunofluorescence co-localization experiments, THP-1 cells were seeded at a density of (1×10^3 cells/well) were inoculated in confocal dishes, and 60 μL of biotin-vitexin (20 μM), and biotin (20 μM) intervened in the incubation for 24 h. The cyto-fluorescence staining process was started. The cells were first washed once with PBS and then fixed with 4% paraformaldehyde for 10 min. the cells were washed three times with PBS, each time for 3 min, and then closed with 5% BSA for 30 min, and diluted with FITC-avidin as well as VDR antibody, and then incubated at 4 ℃ overnight. At the end of the incubation, the cells were washed three times with PBS for 3 min each time, a fluorescent secondary antibody (Alexa Fluor Plus 594) was added, and the cells were incubated for 1 h. The nuclei were washed three times with PBS for 3 min each time, and the nuclei were stained by DAPI for 5 min. After the washing with PBS, the co-localization of the green light and the red light in the cells by laser confocal microscopy was observed.

Molecular docking

The crystal structure of the LBD structural domain (PDB:1QBD) of human VDR was obtained from the Protein Data Bank. Initial structures of ligands and receptors for docking were prepared with MGLTools 1.5.6 (The Scripps Research Institute, CA, USA). Molecular docking was performed with AutoDock Vina 1.0.2. The binding affinity of each docking pose of the oyster glycosides was recovered by the MM/GBSA method in the AmberTools18 software package [33]. Finally, key residues for protein-ligand interactions were identified based on the breakdown energy calculations for each residue.

ChIP-seq and PCR

THP-1 cells were seeded at a density of 4×10^6 in 100 mm dishes. After 24 h, cell attachment was induced by treatment with 100 ng/ml of phorbol 12-myristate 13-acetate (PMA). Subsequently, the cells were preincubated with either dimethyl sulfoxide (DMSO) or vitexin at a concentration of 20 μM for an additional 24 h. Chromatin immunoprecipitation (ChIP) was performed in accordance with the protocol outlined in the Thermo Fisher manual (Catalog No. 26157). Following treatment, THP-1 cells were harvested and crosslinked using 1% paraformaldehyde for 15 min, after which 125 mM glycine was added to quench the crosslinking reaction. Chromatin was sheared into 200–500 bp DNA by sonication using a Biorupter (Diagenode, UCD-200). After reserving 5.0 μl of the sheared chromatin for input to the control samples, the rest of the sheared chromatin was rotationally incubated with 5 μg of VDR (CST, USA, Cat#12550, 1:50) or IgG at 4 °C overnight. The next day, samples were added to protein A/G dynamic beads and incubated at 4 °C for 2 h. The DNA-protein complexes were washed twice with dilution buffer and then eluted from the dynamic beads with SDS buffer. Purified ChIP DNA was obtained after reverse cross-linking, proteinase K digestion, phenol/chloroform extraction, and ethanol precipitation. For ChIP-sequencing, input DNA and ChIP DNA were used to generate sequencing libraries using the Illumina DNA Sample Preparation Kit according to the manufacturer's protocol. Briefly, the DNA samples were end-repaired, then ligated with barcode adapters, and finally amplified and purified. These DNA libraries were sequenced in an Illumina. nextSeq500 sequencer, based on the 35nt pair-end sequencing protocol. Chromatin immunoprecipitation analyses and RNA sequencing were performed with the help of Wuhan GeneBen Biotechnology Co Ltd (Wuhan, China). The promoter primers Cyp24a1 and PBLD were subsequently constructed and detected by RT-PCR.

Luciferase reporter gene assay

HEK293T cells were seeded in 6-well plates at 1×10^5 cells/well, wall-adhered, and transiently transfected with pGL4.10, PGL4.10-CYP24A1, pcDNA3.1-VDR-3×FLAG, and TK-luc using the Lipofectamine 3000 reagent for 6 h. The transfection solution was discarded and added to the high and medium in turn, low concentrations of vitexin (20, 10, and 5 μM) and Calcitriol (50 nM) after induction for 48 h. The transfection solution was washed twice with PBS, and the dual-luciferase reporter gene assay system was used to measure the dual-luciferase activity and to study the effect of vitexin on the transcriptional activation of the CYP24A1 promoter.

Histological assessment

Colon tissues fixed in 4% paraformaldehyde were paraffin-embedded and sectioned were used for histological analysis. The sections were stained with hematoxylin and eosin (H&E) for routine histological evaluation. For immunohistochemistry, sections were deparaffinized and hydrated. Endogenous peroxidase was blocked with 3% H_2O_2 for 30 min. Sections were then incubated with primary antibody at a dilution of 1:100 overnight at 4 °C. Secondary antibodies were incubated at 1:200 for 1 h at room temperature and immunoreactivity was detected by diaminobenzidine (DAB). All sections were counterstained with hematoxylin.

Statistical analysis

All in vitro data represent at least three independent experiments and in vivo data represent at least six independent experiments. All experimental data are expressed as mean ± SEM (standard error of the mean). Statistical analyses were performed using GraphPad Pro Prism 8.0 (GraphPad, San Diego, CA). One-way analysis of variance (ANOVA) followed by Tukey's test was used to analyze differences between groups of data. A p value of <0.05 was considered a significant difference.

Results

VDR plays an important role in the transformation of chronic intestinal inflammation-induced cancer

To systematically and comprehensively identify the key signaling molecules involved in colon cancer, we performed mRNA microarray analysis of intestinal tissues (patients or mice) with CAC and CRC with inflammatory bowel cancer and normal controls and then intersected the previously published dataset to identify differentially expressed genes (DEGs). The results showed that 136 DEGs overlapped across the four datasets. Notably, we found that *Vdr* expression was downregulated in intestinal tissues in these transcriptomic data (Figure S1, Supporting Information). We next performed modeling of chronic intestinal inflammation to carcinoma [25]. As

illustrated in Fig. 1A-C, the duration of this experimental study was 36 days. Post-dissection observations revealed that, in comparison to the control group, the colons of mice in the model group exhibited significant shortening, with tumors of varying sizes emerging at the distal end of the intestine, measuring between 1 and 2 cm. This finding is consistent with atypical hyperplasia characteristic of the intermediate stage of inflammation-initiated carcinogenesis. A comprehensive assessment of the Swiss Volume of Pathology, indicated that the morphology of the terminal intestinal tissues in the model group was markedly disordered, featuring severe disruption of the colonic epithelial barrier, extensive infiltration of inflammatory cells, hyperplasia of submucosal lymphocytes accompanied by lymphoid follicle formation, and structural ambiguity. These observations suggest that the colon tissue during the intermediate modeling stage is undergoing a transition from inflammation to cancer. Genome-wide analyses, along with cellular and animal experiments, have demonstrated that VDR proteins play a role in the prevention of IBD and CRC [34]. As shown in Fig. 1D, VDR protein expression was significantly reduced in the model group compared to the normal group, which is in line with previous studies. In addition, as shown in Fig. 1E, the results of the heatmap indicated that the nuclear transcription gene *Vdr* was significantly decreased compared to the model group. In addition, polarization-related genes such as *ARG1*, *MRC1*, *IL1*, and *Nos2* were also significantly elevated, suggesting that macrophages in the middle stage of CAC were significantly polarized and infiltrated with inflammatory factors (Fig. 1F). Meanwhile, macrophage-polarized expression

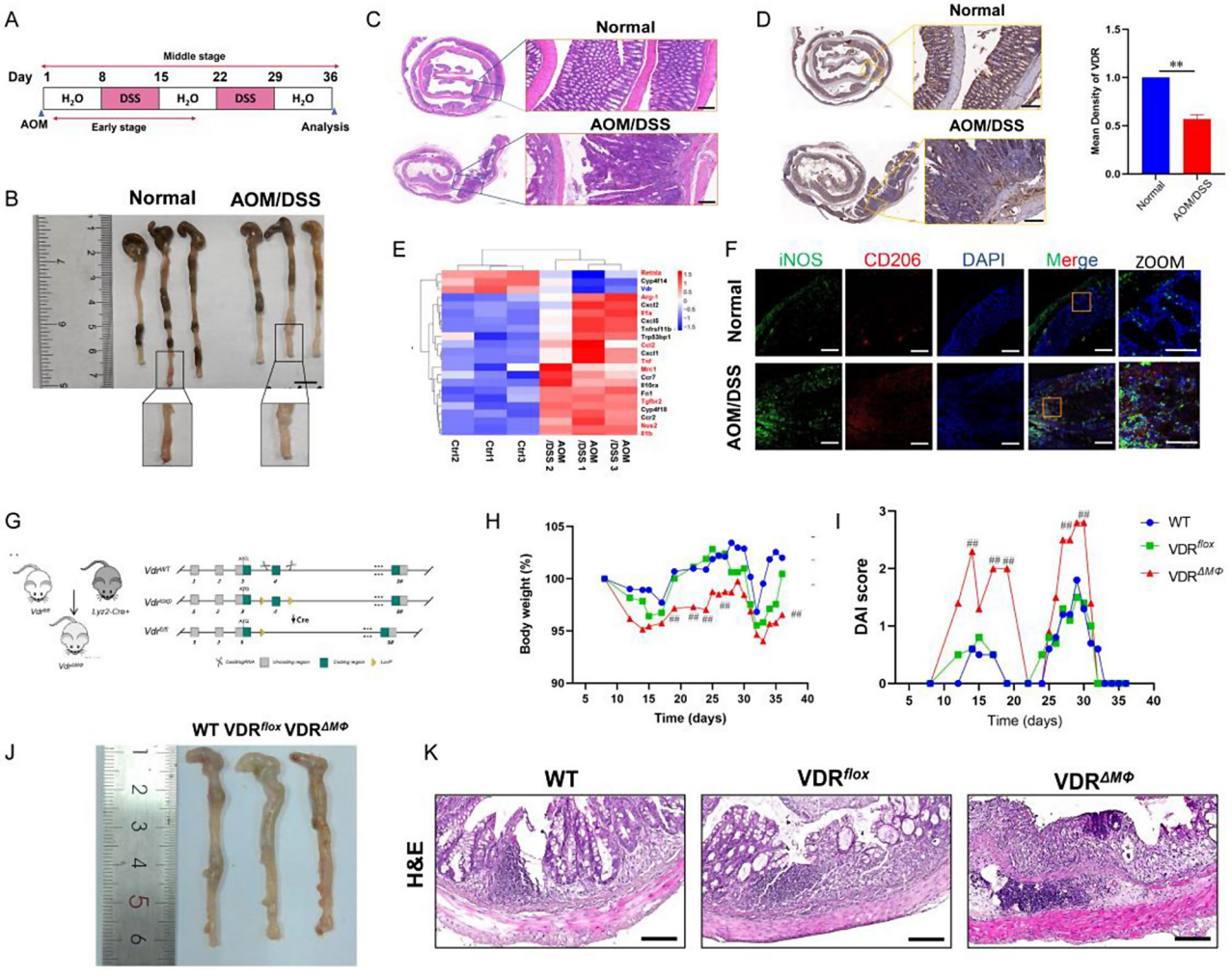

Fig. 1 VDR plays an important role in the transformation of chronic intestinal inflammation-induced cancer. **A**) AOM/DSS induced mid-cycle CAC modeling protocol. **B**) Macroscopic view of colon obtained by mid-stage CAC, Scale bar, 1 cm. **C**) H&E staining of the colon, Scale bar, 200 μm. **D**) Immunohistochemistry of VDR protein and statistics in colon (Scale bar, 100 μm, $^{**}P<0.01$). **E**) Heatmap of the colon. **F**) Immunofluorescence double staining of iNOS and CD206 protein in colon tissue, Scale bar, 100 μm. **G**) Schematic diagram of the experimental design of $VDR^{\Delta M\Phi}$ mice. **H**) Body weight in the mice, $n=6$. **I**) DAI scores, $n=6$. **J**) macroscopic image of the colon. **K**) H&E staining of the colon. The data are presented as the mean ± SEM ($n=3$). $^{\#\#}P<0.01$ vs. WT group

of colonic fluorescence was consistent with transcriptome results.

Most reports suggest that intestinal conditional knockout of host VDR significantly increased tumor formation. We next explored the immunosuppressive role of VDR in the development of murine myeloid knockouts, the construction process of the knockout mouse is shown in Fig. 1G. Western blot analysis showed that colonic tissues of VDR knockout animals displayed a loss of VDR (Figure S2 and S3, Supporting Information), suggesting a successful knockout animal model. We then recorded changes in body weight and DAI in AOM/DSS mice (Fig. 1H-I). As expected, VDR deletion ($VDR^{\Delta M\Phi}$) resulted in significantly slower body weight recovery in AOM/DSS mice, along with significantly higher DAI scores, compared to AOM/DSS controls (WT) and caged controls (VDR^{flox}). Further observation of micro- and macro-colonic tissues showed that the $VDR^{\Delta M\Phi}$ group showed more pronounced colonic barrier disruption and inflammatory infiltration compared to the control group (Fig. 1J-K). These results suggest that VDR plays an important role in the transformation of chronic intestinal inflammation-induced cancer.

Vitexin targets VDR and binds amino acid motifs in its VDR-LBD region to regulate its nuclear transcription

We further investigated whether vitexin could act on the VDR. Cellular thermal shift assay (CETSA), a method for assessing the direct binding of drugs in cells, showed that vitexin, an anti-inflammatory flavonoid, increased the stability of the VDR protein in cells when subjected to a temperature gradient (Fig. 2A). In addition, DARTS experiments showed that vitexin could stabilize the VDR, leading to its increased susceptibility to proteolysis (Fig. 2B). These observations support the possibility that the VDR may serve as a potential cellular target for vitexin. To further confirm the direct binding of vitexin to the VDR, we synthesized a biotin-labeled vitexin probe (Fig. 2C, Figure S4-S6, Supporting Information), and performed immunofluorescence experiments to explore the co-localization of the VDR and biotin-vitexin in THP-1 cells. As shown in Fig. 2D, the VDR (red) showed a clear fluorescence overlap (yellow) with biotin-vitexin (green), suggesting a direct vitexin-VDR interaction in the cells. Altogether, these results suggest that VDR is a direct cellular target of vitexin. Therefore, we further investigated how it regulates VDR. Since the reported small-molecule VDR agonists all bind to the LBD structural domain of the VDR, we suspected that this structural domain might be the site of the vitexin interaction. To verify this experimentally, we constructed prokaryotic proteins of the full-length VDR and the LBD structural domain of the VDR (Figure S7, Supporting Information). Immunoprecipitation pull-down confirmed that biotinylated vitexin interacts with the LBD structural domain of the VDR (Fig. 2E, Figure S8, Supporting Information). Next, we used surface plasmon resonance (SPR) to show that vitexin and VDR-LBD interact with an association rate constant (K_D) of 34.67 μM (Fig. 2F). Finally, we performed isothermal titration calorimetry (ITC) analysis and found that vitexin and VDR-LBD interacted with a binding K_D of 21.07×10^{-5} μM (Fig. 2G). To further determine the structural stability of the binding complex of vitexin and VDR, we performed 100 ns molecular dynamics simulations to determine whether vitexin could exert allosteric modulation on VDR. The results showed that vitexin was able to tighten the VDR structural domain and adjust its conformation (Fig. 2H-I, Figure S9, Supporting Information). In addition, we performed energy decomposition calculations for each of the 11 docking poses in the binding site. We identified 11 residues with low average energies: ALA231, VAL234, SER235, ILE238, MET272, ASN276, THR287, ARG296, THR301, SER306, and ILE314 (Fig. 2J). Of these, we selected THR287 for further study based on their energy values. We transfected HEK 293T cells with wild-type VDR or mutant T287A. Biotinylated vitexin pulled down the wild-type VDR but failed to interact with the mutant VDR (Fig. 2K). These results suggest that THR287 in the LBD structural domain is essential for the interaction of VDR with vitexin.

The VDR protein is implicated in both classical and non-classical signaling pathways, exerting effects through nuclear transcription as well as cytoplasmic interactions. To further elucidate the nuclear import effects of vitexin following VDR targeting, we conducted validation experiments using murine and human-derived macrophages. As illustrated in Fig. 3A, gradient concentrations of both vitexin and calcitriol resulted in an increase in Vdr mRNA levels. Additionally, Fig. 3B presents immunofluorescence data demonstrating the subcellular distribution of VDR protein in the cytoplasm and nucleus following drug treatment. The results indicate that both vitexin and calcitriol significantly enhance VDR protein levels within the nucleus; however, vitexin treatment did not produce a notable increase in cytoplasmic VDR levels, instead promoting its accumulation in the nucleus. We further isolated cytoplasmic and nuclear proteins, confirming that treatment with vitexin and calcitriol facilitated the translocation of VDR proteins into the nucleus (Fig. 3C). In order to measure transcriptional effect, the transcription factor expression plasmid VDR and its CYP24A1 promoter plasmid, were co-transfected into the HEK293T cell. As seen from Fig. 3D, compared with the vector group, the transcription factor VDR was able to activate the target promoter CYP24A1, which was significantly increased after the stimulation by adding increasing concentrations of vitexin and calcitriol, indicating that

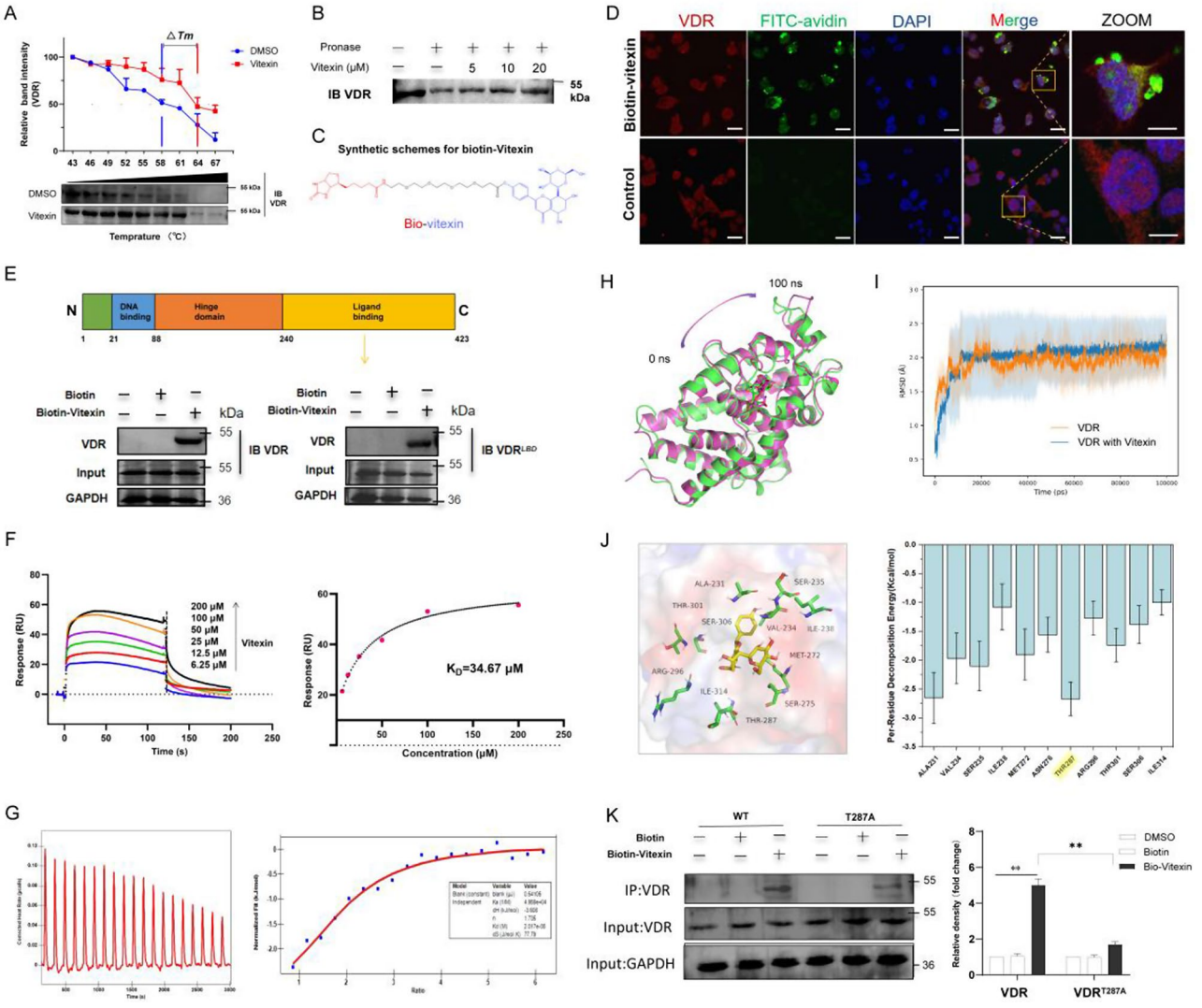

Fig. 2 Vitexin targets VDR and binds amino acid motifs in its VDR-LBD region. **A**) Vitexin promotes the resistance of VDR to different temperature gradients as detected by CETSA in THP-1 cells. **B**) Vitexin enhances the resistance of VDR to proteolytic enzymes as investigated by DARTS. **C**) Chemical structure of Biotin-vitexin (Bio-vitexin). **D**) Co-localization of biotin-vitexin (green) and VDR (red) by immunofluorescence, Scale bar, 10 μm. **E**) Protein blotting analysis of biotin-vitexin binding to the VDR-LBD structural domain. Recombinant proteins VDR and VDR-LBD structural domains were incubated with either biotin- vitexin-loaded magnetic beads or biotin-loaded magnetic beads. The top panel shows the structure of VDR and the bottom panel shows the results of the pulled-down proteins. **F**) SPR analysis showing the interaction between vitexin and recombinant VDR-LBD protein (left). Different concentrations of vitexin were added and K_D values were calculated (right). **G**) ITC analysis of VDR-LBD binding to vitexin, representative images are shown. Representative titration temperature plots are shown on the left, and data integration with the fitted curve (independent model) of vitexin versus VDR-LBD is shown on the right. **H**) The presentative conformation of VDR protein binding with vitexin upon molecular dynamics simulation. **I**) free energy landscape. **J**) The left panel shows the carbon atoms of the side chains of the 11 key residues, with vitexin indicated as green and yellow bars, respectively. The right panel shows a box plot of the per-residue catabolic energy for the 11 residues. **K**) Pull-down analysis of biotin-vitexin binding to mutant VDRs containing T287A. HEK 393T cells were transfected with wild-type VDR or mutants. Lysates were used to assay for binding to biotin-vitexin. The data are presented as the means ± SEM ($n = 3$). **, $P < 0.01$; ns, no significance

vitexin enhances the transcriptional activity of VDR onto CYP24A1 (Figure S14 A-B, Supporting Information). Consistent with the above results, the results of ChIP-PCR showed that the assay results illustrated that both vitexin and calcitriol significantly elevated the expression of CYP24A1 (Fig. 3E). The above experiments confirmed that vitexin binds to amino acid motifs in the VDR-LBD region to enhance the nuclear translocation of VDR, and increases its transcriptional activities.

In the tumor microenvironment, vitexin promotes VDR entry into the nucleus

We subsequently investigated the role of vitexin within the tumor microenvironment. As illustrated in Fig. 4A, we utilized bone marrow-derived macrophages

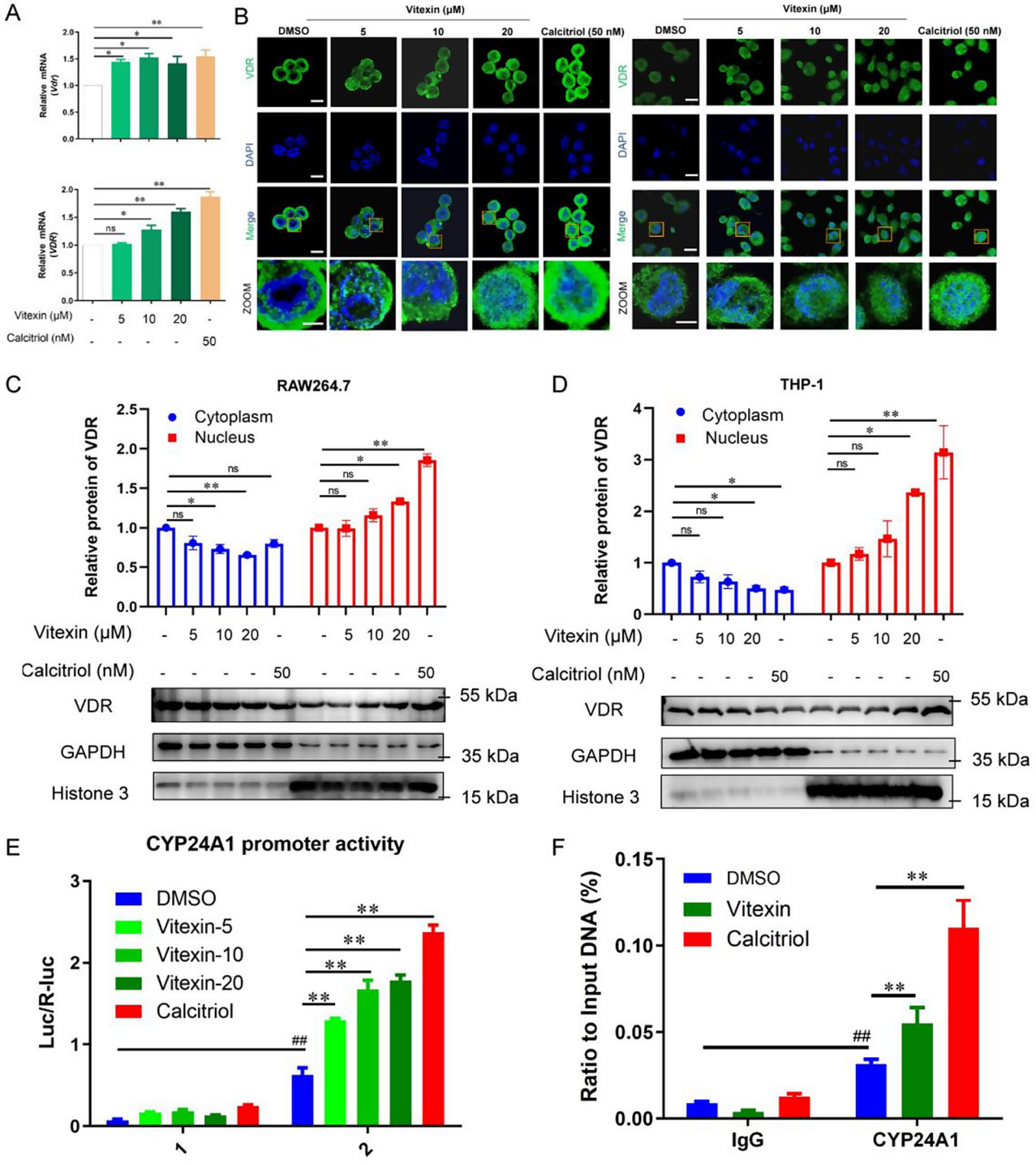

Fig. 3 Vitexin promotes nuclear translocation of VDR protein in macrophages and regulates nuclear transcription. Both RAW264.7 and THP-1 cells were treated with different concentrations of vitexin and Calcitriol. **A**) Gene levels of VDR in RAW264.7 cells (top) and THP-1 cells (bottom) were detected by RT-PCR. **B**) Immunofluorescence was used to examine the levels of VDR in the nucleus and cytoplasm, RAW264.7 cells (left) and THP-1 cells (right). Scale bar, 10 μm. **C-D**) Western blot was used to examine the levels of VDR in the nucleus and cytoplasm. **E**) Detection of transcription factor VDR against CYP24A1 promoter activity using dual luciferase in HEK293T cells. **F**) ChIP-PCR amplification showing VDR activity against the promoter of CYP24A1. The data are presented as the means ± SEM ($n = 3$). *, $P < 0.05$; **, $P < 0.01$; ns, no significance

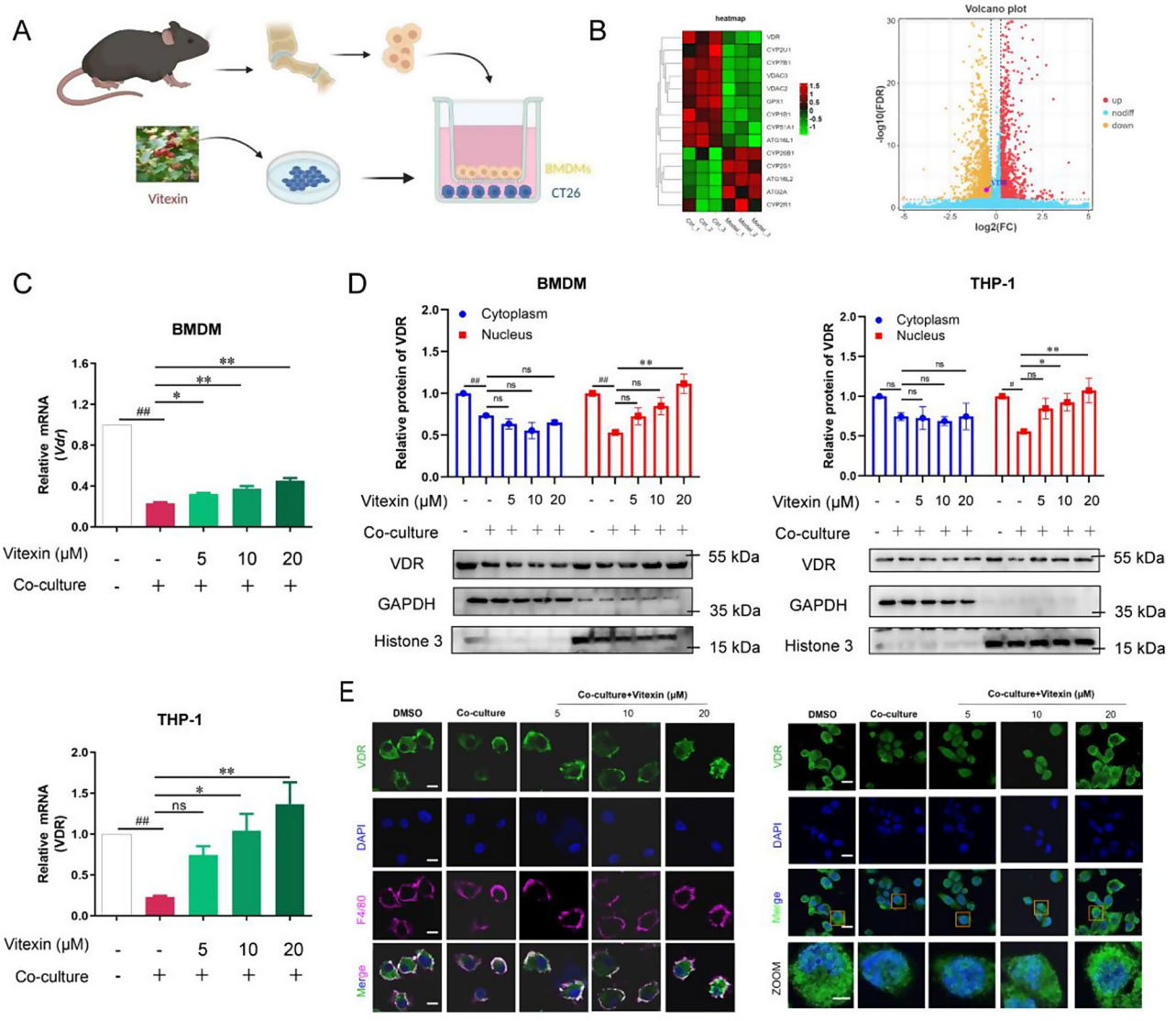

Fig. 4 In the tumor microenvironment, vitexin promotes the nuclear translocation of VDR. **A**) After 48 h incubation with vitexin, CT26 was co-cultured with BMDM for 24 h, which was at the transwell insert, and CT26 was located at the bottom of the cell plate. The experiments related to this section are all co-culture assays. **B**) Left: RNA-seq analysis of THP-1 cells (THP-1 and HCT116) co-cultured with or without treatment with vitexin of differential genes ($n=3$). Right: volcano plot of differential gene enrichment. **C**) Gene levels of VDR in BMDM cells (top) and THP-1 cells (bottom) were detected by RT-PCR. **D**) Western blot was used to examine the levels of VDR in the nucleus and cytoplasm. **E**) Immunofluorescence was used to examine the levels of VDR in the nucleus and cytoplasm. Scale bar, 10 μm. The data are presented as the means ± SEM ($n=3$). $^{\#}$, $P<0.05$; $^{\#\#}$, $P<0.01$; *, $P<0.05$; **, $P<0.01$; ns, no significance

(BMDMs) co-cultured with the homologous intestinal cancer cell line CT26 to simulate the tumor microenvironment for subsequent intervention experiments. Figure 4B demonstrates that following co-culture, the expression of the Vdr gene in the simulated tumor microenvironment was significantly diminished compared to the control group, which aligns with the observed reduction of colon VDR levels in the animal model. PCR analysis revealed a marked decrease in Vdr gene expression after co-culture relative to the normal group; however, treatment with vitexin resulted in a dose-dependent increase in Vdr expression (Fig. 4C). In addition, our results demonstrated that the VDR levels in the cytoplasm and nucleus were reduced after co-culture when compared to the normal group and that the VDR protein in the nucleus was increased in a concentration-dependent manner after the treatment with of vitexin (Fig. 4D). These results were further confirmed by immunofluorescence (Fig. 4E). Together our results suggest that the expression of VDR is significantly reduced in the tumor microenvironment and that the level of VDR in the nucleus increased significantly following treatment with of vitexin.

Vitexin regulates polarization in macrophages in the tumor microenvironment, dependent on VDR

Previous study have confirmed that vitexin upregulates the expression of the M1 type of macrophages in intestinal tissues thereby mitigating intestinal cancer [21]. However, the impact of vitexin on macrophage regulation during the transition from chronic intestinal inflammation to cancer has not been demonstrated. To address this gap, we employed a co-culture system of tumor cells and macrophages to simulate the tumor microenvironment, allowing for a more detailed investigation of the regulatory effects of vitexin on macrophages within this context (Fig. 5A). As shown in Fig. 5B, after treatment with vitexin, we detected macrophage-related genes by real-time PCR and compared the differentially expressed genes in the model or vitexin. As shown in the heatmap, the mRNA levels of *CD163*, *IL1B*, *CCL2*, *IL6*, and *TNF* were significantly increased, while the mRNA level of *MRC1* was significantly decreased, suggesting that vitexin promotes M1 polarization of macrophages in the tumor microenvironment. In addition, we examined the mRNA levels of *Nos2*, *Ccl-2*, *Il-1b*, and *Il-6* in RAW264.7, and the results were consistent with the above trend (Figure S13, Supporting Information). Consistent with the PCR results, the results of flow cytometry also showed that in the tumor microenvironment, vitexin regulated macrophage M1 polarization in a dose-dependent manner, while M2-polarised macrophages were significantly decreased (Fig. 5C-D). Next, we used VDR knockdown macrophages to reverse validate the role of vitexin in regulating macrophages (Fig. 5E). It was found by flow cytometry results (Fig. 5F-G) that the macrophage-regulating effect of vitexin was eliminated in the VDR-knockdown cell model, however, the control treatment group was expressed consistent with the above results. Meanwhile, there was no significant change in the mRNA levels of *Nos2* and *Arg-1* by vitexin in BMDM cells with VDR knocked down (Fig. 5H), suggesting that vitexin could regulate macrophage polarization but is dependent on VDR.

Vitexin regulates macrophage polarization in the tumor microenvironment via the VDR/PBLD pathway

Our findings suggest that Vitexin can regulate macrophage polarization through VDR protein. Next, we further explored which genes are regulated by VDR to regulate macrophage polarization. Co-cultured THP-1 cells using ChIP-Seq data are shown with high-resolution peaks identified in the read density (Fig. 6A-B, Figure S14 C-D, Supporting Information). Guided by the ChIP-Seq results, further ChIP-PCR experiments were performed to confirm the binding regions. A series of primers were designed for the genomic fragments surrounding the transcription start site. Real-time fluorescence quantitative PCR analysis of immunoprecipitated DNA showed that the P1 (-310/-290 bp) and P2 (-327/-313 bp) fragments were the most enriched (Fig. 6C), suggesting that the P1 and P2 fragments may contribute to the vitexin-regulated VDR regulation of PBLD transcription. Based on the ChIP results, a series of luciferase reporter genes driven by different PBLD gene fragments were constructed. Based on bioinformatics analysis, we deleted two VDRE sites in specific intervals of the PBLD promoter and examined the effect of VDR on the transcriptional activity of the PBLD promoter (Fig. 6D). Mutation 2 significantly attenuated the enhancing effect of VDR, whereas mutation 1 had no effect (Fig. 6E). These results suggest that VDR can enhance PBLD transcription by directly binding to the P1 fragment of the PBLD promoter. The VDR was significantly increased following stimulation with vitexin, indicating that vitexin may enhance the activation of the PBLD promoter by VDR. Previous studies have demonstrated that epithelial PBLD plays a role in mitigating intestinal inflammatory responses and enhancing intestinal barrier function, potentially through the inhibition of the NF-κB signaling pathway [35]. However, whether it affects macrophage polarization has not been reported. Weknocked down the PBLD protein in THP-1 cells (Fig. 6F) and analyzed the effects by flow cytometry and PCR. The results showed that the ability to regulate macrophages disappeared in the siPBLD group compared with the control group after vitexin treatment (Fig. 6G-H). Meanwhile, there was no significant change in the mRNA levels of *iNOS2* and *ARG-1* by vitexin in THP-1 cells with VDR knocked down (Fig. 6I). Overall, the regulation of macrophage polarization by vitexin in the tumor microenvironment is dependent on the VDR-PBLD pathway.

In vivo, vitexin mitigates the transition from chronic intestinal inflammation to cancer by modulating macrophage polarization and is dependent on the VDR/PBLD pathway

The above results in vitro demonstrated that vitexin modulates the VDR/PBLD pathway to regulate macrophage polarization in the tumor microenvironment. We constructed mid-CAC mice and administered vitexin intervention. As shown in Fig. 7A-B, all mice in the mid-stage CAC group had significantly decreased body weight compared with the normal group. In animals with normal macrophage VDR expression (VDR^{flox}), the body weights of animals in both calcitriol and vitexin intervention groups were significantly increased, however, in animals with macrophage VDR deletion ($VDR^{\Delta M\Phi}$), administration of the intervention groups did not have an effect, and the body weights of the animals were not affected compared to the CAC group. As shown in Fig. 7C, in the VDR^{flox} group, the body weight DAI of mice in the

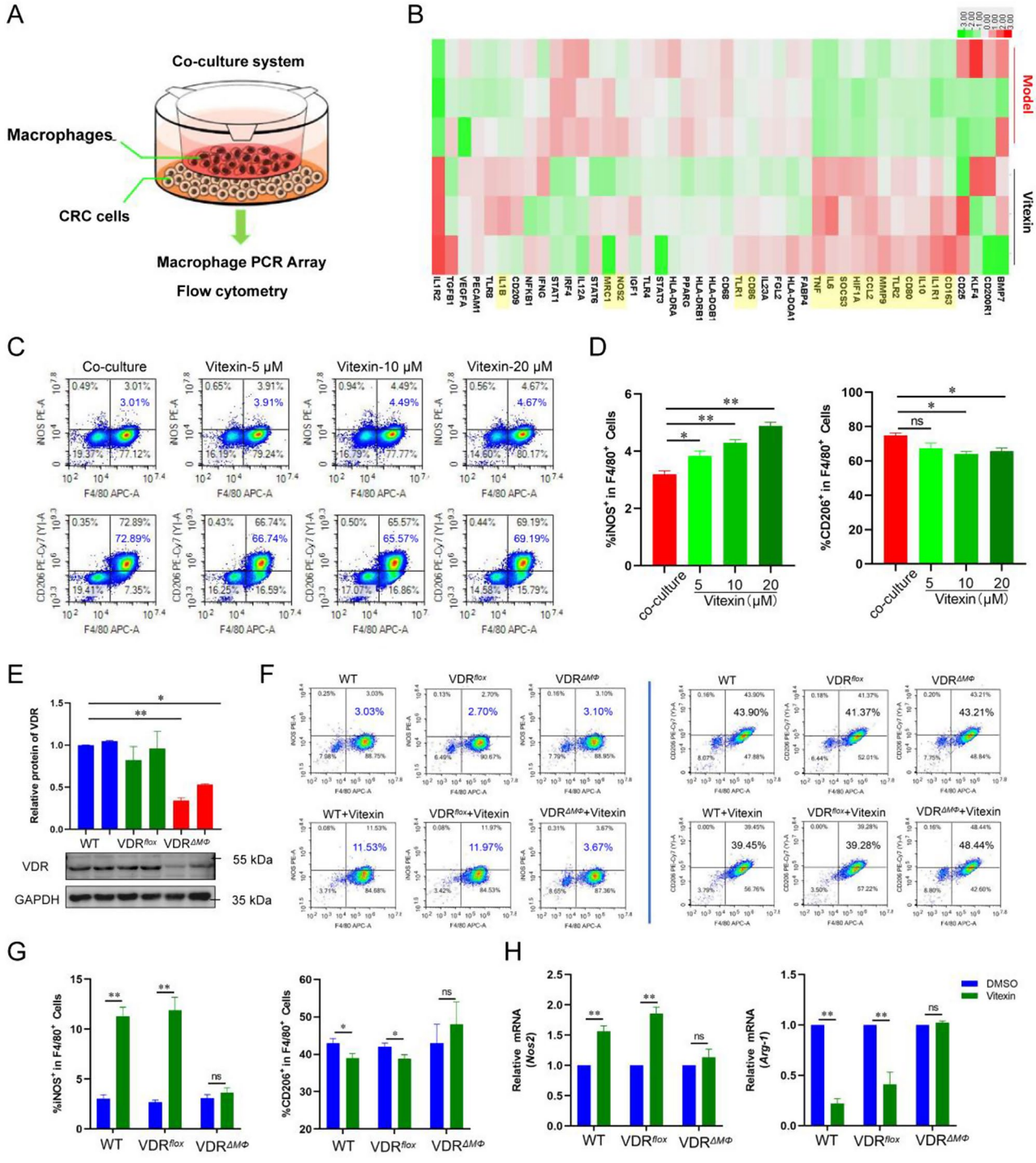

Fig. 5 Vitexin regulates polarization in macrophages in co-culture, dependent on VDR. **A**) Schematic diagram of the in vitro Transwell-based coculture system. **B**) Heatmap of gene expression levels detected in macrophage arrays of co-cultured THP-1 cells for 24 h with or without vitexin treatment ($n = 3$ each). **C**) Data are presented as representative FACS plots. **D**) Flow cytometry analysis of iNOS or CD206 levels in BMDM cells from WT mice. **E**) Western blot detection of VDR expression in BMDM from WT, VDR^{flox}, and VDR$^{\Delta M\Phi}$. **F**) Flow cytometry analysis of iNOS or CD206 levels in BMDM cells. **G**) Data are presented as representative FACS plots and in summary plots. **H**) The levels of *Nos2* and *Arg-1* mRNA. The data are presented as the mean ± SEM ($n = 3$). *, $P < 0.05$; **, $P < 0.01$; ns, no significance

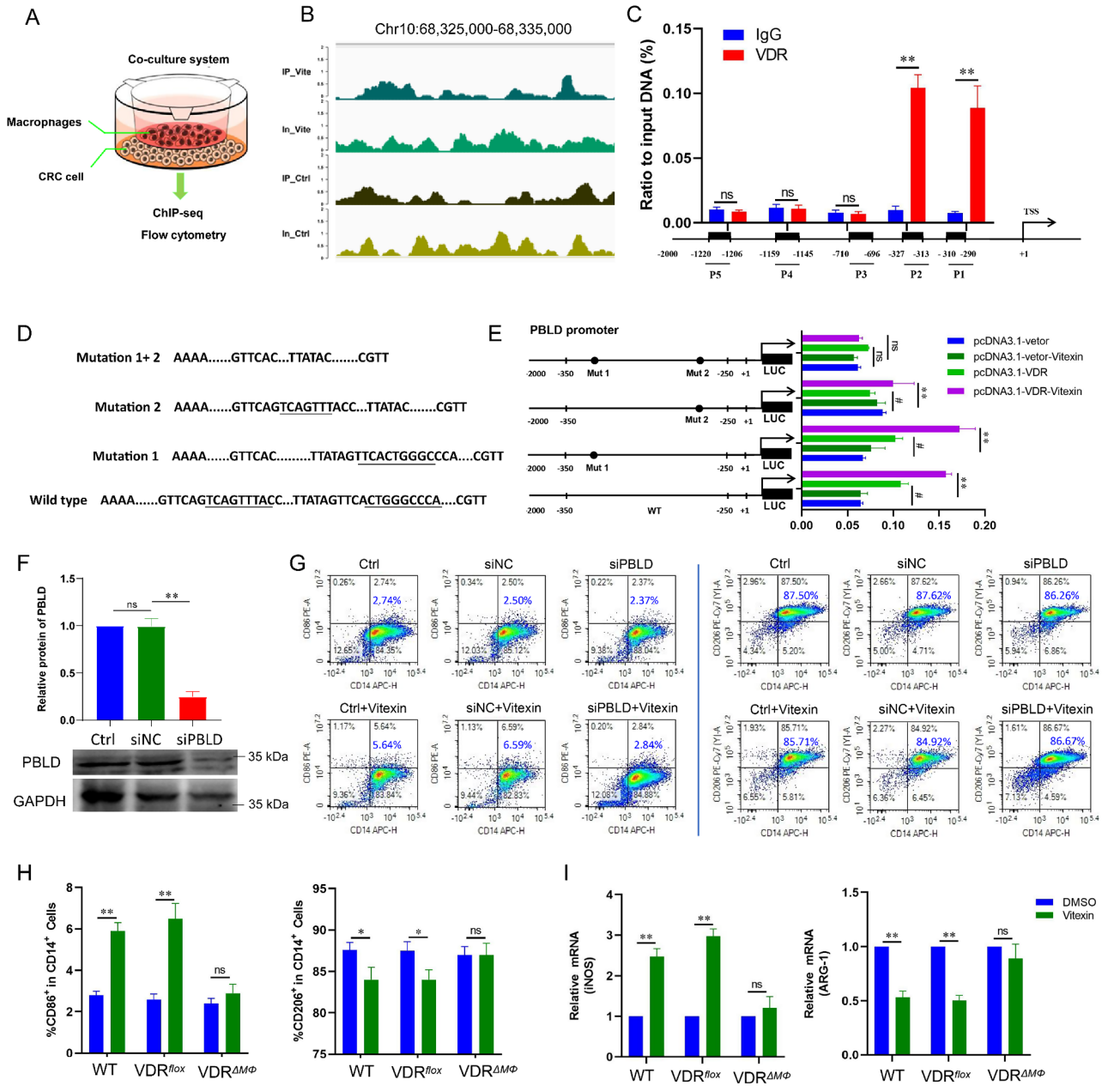

Fig. 6 Vitexin regulates macrophage polarization in the tumor microenvironment via the VDR/PBLD pathway. **A**) Schematic diagram of the in vitro Transwell-based coculture system. **B**) Binding maps of VDR to the PBLD gene were analyzed from ChIP-Seq data in the control and vitexin groups and visualized by IGV software. **C**) The abundance of gene fragments in the input and immunoprecipitates was evaluated using designated primers through real-time PCR, and the position of the primers was detected by ChIP. **D**) Schematic representation of the PBLD promoter containing three VDREs, with the promoter's mutation strategy shown in the figure. **E**) Transcriptional regulatory activity of VDR on full-length PBLD promoter and doubly VDRE-mutated PBLD promoter in HEK293T cells with or without Vitexin treatment measured by dual-luciferase reporter gene assay. **F**) Western blot assay for VDR expression. **G**) Flow cytometry analysis of CD86 and CD206 levels. Data are presented as representative FACS plots. **H**) Statistical results of macrophage typing. **I**) mRNA levels of INOS and ARG-1. Data are expressed as SEM ± mean ($n = 3$). $^{\#}$, $P < 0.05$; $^{\#\#}$, $P < 0.01$; *, $P < 0.05$; **, $P < 0.01$; ns, no significance

mid-term CAC group was significantly increased compared to the normal group, but the DAI was significantly decreased after intervention with both calcitriol and vitexin. However, in the $VDR^{\Delta M\Phi}$ group, the administered intervention group did not have an intervention effect, and the animals' DAI was not changed compared with the CAC group. As shown in Fig. 7D, compared with the normal group, the colons of mice in the model group had different degrees of shortening, swelling, and a little tumor-like growth. As shown in Fig. 7E-F, in the VDR^{flox} group, the length of the colon was significantly longer and the thickness was significantly decreased after

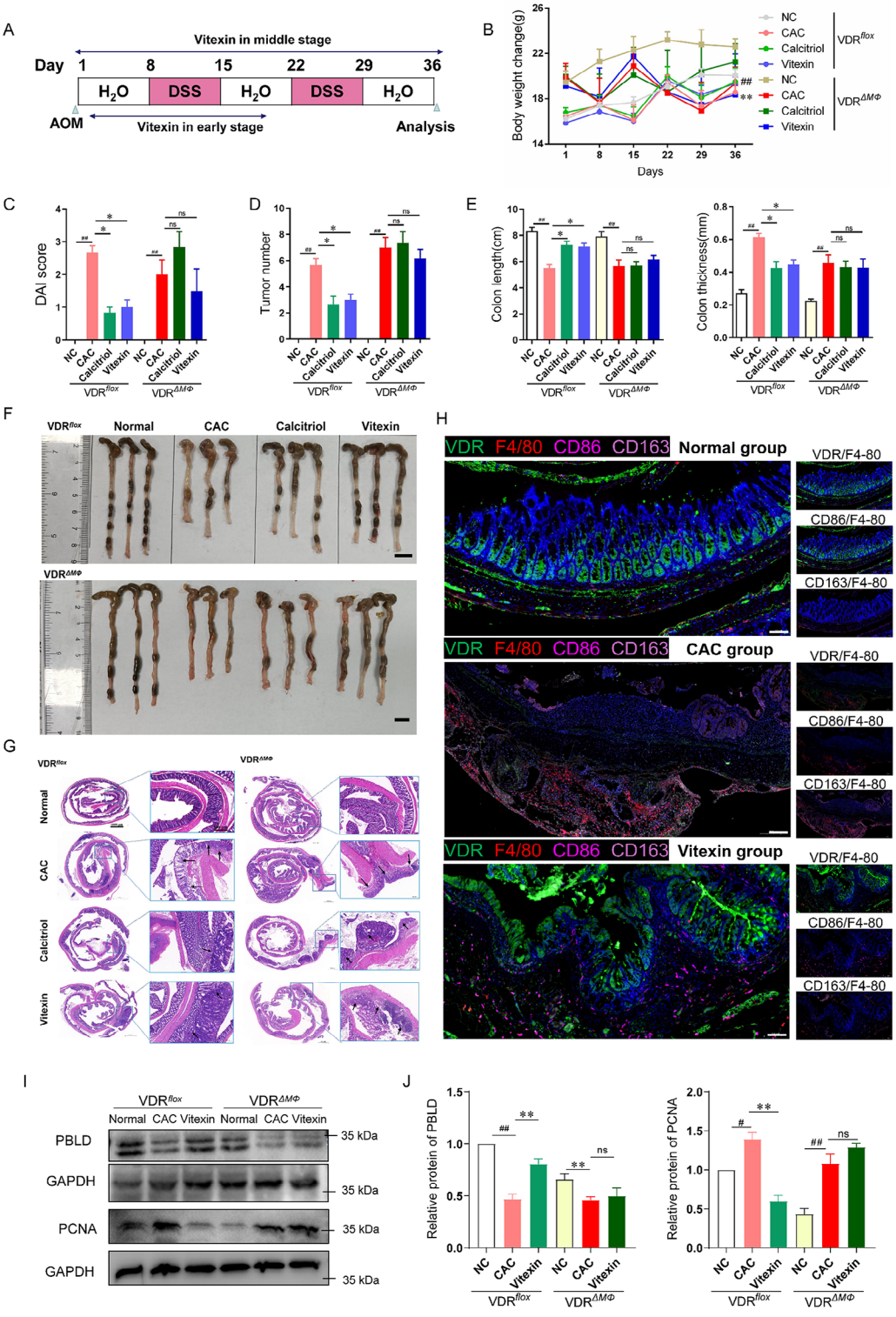

Fig. 7 Vitexin mitigates the transition from chronic intestinal inflammation to cancer by modulating macrophage polarization and is dependent on the VDR/PBLD pathway. **A**) Flow chart of drug administration. **B**) Graph of body weight changes (The data are presented as the means ± SEM ($n = 6$). In the VDR^{flox} group, $^{\#\#}P < 0.01$ compared with the NC group and $^{**}P < 0.01$ compared with the CAC group.). **C**) DAI score. **D**) Tumor number. **E**) Colon length (left), colon thickness (right). **F**) Macroscopic view of colon, Scale bar, 1 cm. **G**) H&E staining of the colon, Scale bar: 1000 μm and 200 μm, $n = 3$). **H**) Multicolour immunohistochemistry of colon tissue (VDR-green, F4/80 red, CD86 pink, CD163 rose. Scale bar, 500 μm, $n = 3$). **I-J**) The expression of PBLD and PCNA proteins and statistical plots ($n = 3$). The data are presented as the means ± SEM ($n = 6$). $^{\#}P < 0.05$, $^{\#\#}P < 0.01$;$^{*}P < 0.05$, $^{**}P < 0.01$; ns, no significance

the treatment with calcitriol and vitexin compared with the model group. The number of tumors was significantly reduced after calcitriol treatment, but there was no significant difference for vitexin. In addition, as shown in the colon pathogram (Fig. 7G), the inhibitory effect of vitexin on the development of colorectal cancer was not significant in the $VDR^{\Delta M\Phi}$ group. This suggests that vitexin inhibits colorectal cancer development through VDR. In the $VDR^{\Delta M\Phi}$ group, there was a loss of tissue morphology in the marginal zone of colorectal cancer, with disturbed cell arrangement, necrosis, and hyperplasia. In the VDR^{flox} group, the intervention of vitexin was able to reduce the hyperplasia of the cancerous zone and improve the tissue morphology, whereas the improvement of the cancerous zone by vitexin was not significant in the $VDR^{\Delta M\Phi}$ group, which indicated that the improvement of cancerous cell hyperplasia by vitexin in the cancerous zone relied on the VDR proteins. We employed multi-immunohistochemistry techniques, as illustrated in Fig. 7H, to analyze colonic tissues from normal mice. The results indicated that the normal group exhibited abundant expression of VDR proteins, while the phenotypic expression of macrophage cells was notably low. In contrast, macrophages in the model group displayed significant polarization and markedly reduced levels of VDR compared to the normal group. However, following vitexin administration, there was a significant increase in both VDR and CD163 levels, suggesting that vitexin upregulates VDR protein and modulates macrophage polarization towards the M1 phenotype. Consistent with these findings, western blot analysis revealed that the expression of PBLD and PCNA proteins was significantly decreased in the CAC group compared to the normal group. Notably, after vitexin treatment, the expression levels of PBLD and PCNA proteins in the colon tissues of unknocked-out VDR mice approached those observed in normal mice (Fig. 7I-J). However, for the tissues of mice with knockout VDR, the above proteins did not change significantly after vitexin treatment (Fig. 7I-J). In conclusion, vitexin mitigates the transition from chronic intestinal inflammation to cancer by modulating macrophage polarization and is dependent on the VDR/PBLD pathway.

Discussion

Chronic colitis is recognized as a significant risk factor for the development of colitis-associated cancer, which typically progresses through a sequence of inflammation, typical hyperplasia, and subsequent cancerization. This progression involves a transition of the lesion microenvironment from an inflammatory state to a tumor-promoting microenvironment. In this study, we specifically targeted the VDR to modulate macrophage polarization, demonstrating that vitexin can inhibit the transition from chronic colitis to CAC. Our findings indicate that vitexin binds to the VDR protein, thereby preventing the differentiation of macrophages into the M2 phenotype and preserving the cytotoxic effects of inflammatory cytokines produced by M1-type macrophages. In vitro coculture experiments revealed that vitexin increased the proportion of M1-type macrophages, supporting its anticancer properties. Furthermore, we employed myeloid-specific VDR gene knockout mice to elucidate the critical role of VDR in the mid-term progression of CAC and to confirm the targeting of VDR by vitexin. These key findings are illustrated in the graphical abstract.

One of the most important contributions of this study may be the discovery of a natural product - vitexin, which is a novel VDR agonist. Vitexin, as a flavonoid active substance, has been reported to have therapeutic effects on many cancers, including breast cancer, cervical cancer, and many other cancers [36–38]. Our previous studies have also confirmed that vitexin can alleviate the disease in UC and CAC mice, suggesting that vitexin may have a broad effect on cancers associated with the evolution of colitis [21, 39]. However, the molecular mechanisms and targets of vitexin remain unknown, limiting the application of vitexin.

VDR, a nuclear receptor transcription factor, has been investigated in clinical and basic studies for its important role in colitis and colorectal cancer [40–43]. Studies have correlated vitamin D with survival and mortality in colorectal cancer, and in a large group of CRC patients, higher VDR expression in tumor stromal fibroblasts was associated with longer survival [44]. In the present study, it was also confirmed that mid-stage CAC mice with VDR on the table of CAC mice deficient in VDR showed more severe colon lesions and accelerated their cancerous process compared to control mice. These results suggest that VDR is a potential therapeutic target. However, one of the most promising vitamin D analogs, seocalcitol, has not demonstrated efficacy in phase II clinical trials [45]. Recent findings suggest that the relationship between elevated vitamin D levels and a reduced risk of colorectal cancer is not universally supported. Additionally, systemic activation of vitamin D signaling poses a potential risk of hypercalcemia, which can lead to severe toxicity. Notably, this study identifies vitexin as a novel agonist of the vitamin D receptor (VDR), demonstrating its ability to bind directly to the ligand-binding domain of VDR. The interaction between vitexin and VDR is significantly influenced by the residue THR-287 within the VDR structural domain, which may facilitate the design and development of new small-molecule VDR agonists. Furthermore, our findings indicate that vitexin markedly upregulates the transcription of VDR's classical target gene, Cyp24a1. However, the implications of vitexin on the overall targeting of VDR during the CAC process,

following VDR's translocation to the nucleus, warrant further investigation.

Previous studies have shown that vitexin can alleviate the condition of CAC mice by regulating the polarization of macrophages, but its mechanism has not been thoroughly studied. As a novel VDR agonist, it is unknown whether vitexin is related to macrophage polarization. Therefore, we used an in vitro co-culture method to simulate the regulatory effect of vitexin on macrophages in the tumor microenvironment. The results found that vitexin can upregulate the content of VDR in the nucleus of macrophages, promote its entry into the cell nucleus, upregulate the polarization of M1-type macrophages, and downregulate the polarization of M2-type macrophages. However, when we extracted VDR knockout cells for further verification, we found that in macrophages with VDR knockout, vitexin could not exert its regulatory effect on macrophage polarization, indicating that the regulation of vitexin on macrophage polarization depends on VDR protein. Recent studies have confirmed that VDR-deficient keratinocyte-derived exosome miR-4505 promotes macrophage polarization towards the M1 phenotype, and that VDR can mediate hepatic ischemia-reperfusion injury by regulating M2 macrophage polarization through autophagy [46, 47]. However, how vitexin affects VDR and thus regulates macrophage polarization is not yet known.

Genomics and proteomics data have shown that PBLD expression is deficient in a variety of tumors. PBLD is expressed in the liver, stomach, mammary gland, kidney, and intestine, and acts as a tumor suppressor in gastric carcinoma [48], hepatocellular carcinoma [49, 50], and breast cancer [51]. acting as a tumor suppressor. The inhibitory role of PBLD in cancer is relatively clear; however, little is known about the role of PBLD in macrophage polarization, especially in CAC. A previous study demonstrated that PBLD levels were significantly reduced in UC and that PBLD expression levels were negatively correlated with UC severity, inhibiting NF-κB and epithelial-mesenchymal transition signaling pathways and acting as a tumor suppressor [35]. We report, for the first time, that the VDR directly binds to the −310/-290 promoter region of the PBLD gene, thereby promoting its transcription and expression. Following treatment with vitexin, we observed a significant increase in the transcriptional expression of PBLD, indicating that vitexin enhances PBLD expression. Subsequently, we knocked down PBLD expression in THP-1 cells within the tumor microenvironment and found that the regulatory effect of vitexin on macrophage polarization was abolished. These findings demonstrate that vitexin can modulate macrophage polarization in the tumor microenvironment, with this effect being dependent on the VDR/PBLD signaling pathway.

In this study, we generated bone marrow-specific VDR gene knockout mice, which demonstrated an accelerated progression of colorectal cancer. These findings provide compelling evidence that VDR may serve as a potential target for preventing the transition from colitis to colorectal cancer. Notably, we observed that the absence of VDR in colitis-associated colorectal cancer (CAC) mice during mid-term treatment with vitexin did not yield therapeutic effects, nor did we detect any modulation of macrophage polarization by vitexin. A limitation of this study may be the lack of evaluation of VDR expression in specific intestinal macrophage populations. Although VDR expression in the intestine is relatively low, its expression in intestinal macrophages is significant, underscoring VDR's critical role in intestinal immunity.

Conclusion

In conclusion, our findings indicate a significant reduction in the expression of VDR protein in mid-term CAC mice, with the absence of VDR protein appearing to accelerate the progression of CAC. This acceleration is likely attributable to alterations in macrophage polarization. Vitexin has been shown to directly target VDR, binding to the VDR-LBD structural domain, which facilitates its translocation into the cell nucleus. This process subsequently regulates the transcription of PBLD and influences macrophage polarization. These results underscore the direct targeting capability of vitexin and highlight the critical role of VDR as a key pathogenic factor in the transition from colitis to colorectal cancer. Furthermore, our study supports the potential for future research and the application of vitexin in preventing the progression from colitis to colorectal cancer.

Abbreviations

AOM	Azoxymethane
BMDM	Bone marrow-derived macrophage
CAC	Colitis associated cancer
CETSA	Cellular heat transfer assay
CRC	Colorectal cancer
DARTS	Drug affinity responsive target stability
DSS	Dextran sulfate sodium salt
ITC	Isothermal Titration Calorimetry
MΦ	Macrophage
PBLD	Phenazine biosynthesis like protein domain
SPR	Surface plasmon resonance assay
TME	Tumor microenvironment
VDR	Vitamin D receptors
WT	Wild type

Supplementary Information

The online version contains supplementary material available at https://doi.org/10.1186/s12943-024-02108-6.

Supplementary Material 1

Supplementary Material 2

Author contributions
Y. C., J. L and S. C. designed, performed, and analyzed experiments, and wrote the manuscript. N. L., and X.S. designed and analyzed experiments. J.Z. and C. C. designed image analysis and provided intellectual input. Y.C. and X.Y. designed and performed statistical and image analysis. Z. X., M. C. and E. Z. assisted with image acquisition and designed image analysis. M. C., S. W., S. H. and H. T. directed the study, designed and analyzed experiments, and wrote the manuscript.

Funding
This work was supported by the Open Subjects of State Key Laboratory of Dampness Syndrome of Chinese Medicine jointly established by the Ministry of Provincial Affairs of the People's Republic of China; National Natural Science Foundation of China (82304905, 82272326); Natural Science Foundation of Guangdong Province (2023A1515011729, 2022A1515012408); Foundation and Applied Basic Research Fund Project of Guangdong Province (2021B1515140045 and 2021B1515140050), Guangzhou Science and Technology Bureau (202102080643), Science and Technology Program of Guangzhou (202002020032), The core technology project in the field of biological industry (2021ZD006), Regional Union Fund-Regional Nurturing Project (2021B1515140065), and Science and technology project in key fields of Nansha District (2022ZD004), the Open Project of State Key Laboratory of Respiratory Disease (SKLRD-OP-202202 and SKLRD-OP-202317); the Guangzhou Medical University Discipline Construction Funds (Basic Medicine) (JCXKJS2022A11).

Data availability
No datasets were generated or analysed during the current study.

Declarations

Ethics approval and consent to participate
All mouse experiments were approved by the Animal Ethics Committee of the NKI and were performed according to institutional and national guidelines.

Competing interests
The authors declare no competing interests.

Author details
[1]School of Basic Medical Sciences, State Key Laboratory of Respiratory Disease, Sino-French Hoffmann Institute, Guangzhou Medical University; The Affiliated Panyu Central Hospital of Guangzhou Medical University; Guangdong Provincial Key Laboratory of Allergy & Clinical Immunology, The Second Affiliated Hospital of Guangzhou Medical University, Guangzhou, Guangdong 511436, China
[2]State Key Laboratory of Dampness Syndrome of Chinese Medicine, The Second Affiliated Hospital of Guangzhou University of Chinese Medicine; School of Pharmaceutical Sciences, Guangzhou University of Chinese Medicine, Guangzhou, Guangdong 510006, China
[3]Department of Hepatobiliary Surgery, The Third Affiliated Hospital of Sun Yat-Sen University, Guangzhou 510000, China
[4]Department of Pharmacy, The Second Affiliated Hospital of Guangzhou, University of Chinese Medicine, Guangzhou 510120, China
[5]State Key Laboratory of Oncology in South China Guangdong Provincial Clinical Research, Center for Cancer Sun Yat-Sen University Cancer Center Guangzhou, Guangzhou 510060, China
[6]Clinical Medical College of Acupuncture Moxibustion and Rehabilitation, Guangzhou University of Chinese Medicine, Guangzhou, Guangdong 510006, China

Received: 1 July 2024 / Accepted: 2 September 2024
Published online: 13 September 2024

References

1. Zhang L, Li Z, Skrzypczynska KM, Fang Q, Zhang W, O'Brien SA, He Y, Wang L, Zhang Q, Kim A, et al. Single-cell analyses inform mechanisms of myeloid-targeted therapies in Colon cancer. Cell. 2020;181:442–+.
2. Fujita M, Matsubara N, Matsuda I, Maejima K, Oosawa A, Yamano T, Fujimoto A, Furuta M, Nakano K, Oku-Sasaki A, et al. Genomic landscape of colitis-associated cancer indicates the impact of chronic inflammation and its stratification by mutations in the wnt signaling. Oncotarget. 2018;9:969–81.
3. Wang X, Chen JDZ. Therapeutic potential and mechanisms of sacral nerve stimulation for gastrointestinal diseases. J Translational Intern Med. 2023;11:115–27.
4. Xu Y, Liu K, Li C, Li M, Liu F, Zhou X, Sun M, Ranganathan M, Zhang L, Wang S et al. The largest Chinese cohort study indicates homologous recombination pathway gene mutations as another major genetic risk factor for colorectal Cancer with heterogeneous clinical phenotypes. Research 2023, 6.
5. Yaeger R, Shah MA, Miller VA, Kelsen JR, Wang K, Heins ZJ, Ross JS, He Y, Sanford E, Yantiss RK, et al. Genomic alterations observed in Colitis-Associated Cancers are distinct from those found in sporadic colorectal cancers and vary by type of inflammatory bowel disease. Gastroenterology. 2016;151:278–.
6. Ma X, Meng Z, Jin L, Xiao Z, Wang X, Tsark WM, Ding L, Gu Y, Zhang J, Kim B, et al. CAMK2γ in intestinal epithelial cells modulates colitis-associated colorectal carcinogenesis via enhancing STAT3 activation. Oncogene. 2017;36:4060–71.
7. Xu R, Du A, Deng X, Du W, Zhang K, Li J, Lu Y, Wei X, Yang Q, Tang H. tsRNA-GlyGCC promotes colorectal cancer progression and 5-FU resistance by regulating SPIB. J Exp Clin Cancer Res. 2024;43:230.
8. Saeed H, Leibowitz BJ, Zhang L, Yu J. Targeting myc-driven stress addiction in colorectal cancer. Drug Resist Updates 2023, 69.
9. Xing P, Wang S, Cao Y, Liu B, Zheng F, Guo W, Huang J, Zhao Z, Yang Z, Lin X et al. Treatment strategies and drug resistance mechanisms in adenocarcinoma of different. Drug Resist Updates 2023, 71.
10. Wu S, Yan M, Liang M, Yang W, Chen J, Zhou J. Supramolecular host-guest nanosystems for overcoming cancer drug resistance. Cancer drug Resist (Alhambra Calif). 2023;6:805–27.
11. Rainho MA, Siqueira PB, de Amorim ISS, Mencalha AL, Thole AA. Mitochondria in colorectal cancer stem cells - a target in drug resistance. Cancer drug Resist (Alhambra Calif). 2023;6:273–83.
12. Jiang Z, Zou Q, Chen Q, Zhang J, Tang H, Chen J, Qin Y, Yang L, Chen Z, Cao L. Therapeutic role of Wuda granule in gastrointestinal motility disorder through promoting gastrointestinal motility and decreasing inflammatory level. Front Pharmacol 2023, 14.
13. Wu B, Shi X, Jiang M, Liu H. Cross-talk between cancer stem cells and immune cells: potential therapeutic targets in the tumor immune microenvironment. Mol Cancer 2023, 22.
14. Yuan Z, Li Y, Zhang S, Wang X, Dou H, Yu X, Zhang Z, Yang S, Xiao M. Extracellular matrix remodeling in tumor progression and immune escape: from mechanisms to treatments. Mol Cancer 2023, 22.
15. Xiang D, Jiang L, Yuan Q, Yu Y, Liu R, Chen M, Kuai Z, Zhang W, Yang F, Wu T et al. Leukocyte-specific morrbid promotes leukocyte differentiation and atherogenesis. Research 2023, 6.
16. Yang W, Ma Y, Xu H, Zhu Z, Wu J, Xu C, Sun W, Zhao E, Wang M, Reis RL et al. Mulberry uiomass-derived nanomedicines mitigate colitis through improved inflamed mucosa accumulation and intestinal microenvironment modulation. Research 2023, 6.
17. Zhang H, Wang X, Zhang J, He Y, Yang X, Nie Y, Sun L. Crosstalk between gut microbiota and gut resident macrophages in inflammatory bowel disease. J Translational Intern Med. 2023;11:382–92.
18. Lu J, Li J, Lin Z, Li H, Lou L, Ding W, Ouyang S, Wu Y, Wen Y, Chen X et al. Reprogramming of TAMs via the STAT3/CD47-SIRPα axis promotes acquired resistance to EGFR-TKIs in lung cancer. Cancer Lett 2023, 564.
19. Wang Z, Wang S, Jia Z, Hu Y, Cao D, Yang M, Liu L, Gao L, Qiu S, Yan W et al. YKL-40 derived from infiltrating macrophages cooperates with GDF15 to establish an immune suppressive microenvironment in gallbladder cancer. Cancer Lett 2023, 563.
20. Shan H, Dou W, Zhang Y, Qi M. Targeted ferritin nanoparticle encapsulating CpG oligodeoxynucleotides induces tumor-associated macrophage M2 phenotype polarization into M1 phenotype and inhibits tumor growth. Nanoscale. 2020;12:22268–80.
21. Chen Y, Wang B, Yuan X, Lu Y, Hu J, Gao J, Lin J, Liang J, Hou S, Chen S. Vitexin prevents colitis-associated carcinogenesis in mice through regulating macrophage polarization. Phytomedicine 2021, 83.
22. Abreu MT, Kantorovich V, Vasiliauskas EA, Gruntmanis U, Matuk R, Daigle K, Chen S, Zehnder D, Lin YC, Yang H, et al. Measurement of vitamin D levels in inflammatory bowel disease patients reveals a subset of Crohn's disease patients with elevated 1,25-dihydroxyvitamin D and low bone mineral density. Gut. 2004;53:1129–36.
23. Song M, Chan AT, Sun J. Influence of the gut microbiome, diet, and environment on risk of colorectal cancer. Gastroenterology. 2020;158:322–40.

24. Knackstedt R. The Importance of vitamin D, the vitamin D receptor (VDR) and retinoid X receptor alpha (RXRα) in murine colitis development and progression. *Dissertation/Thesis*. 2013.
25. Levi-Galibov O, Lavon H, Wassermann-Dozorets R, Pevsner-Fischer M, Mayer S, Wershof E, Stein Y, Brown LE, Zhang W, Friedman G et al. Heat shock factor 1-dependent extracellular matrix remodeling mediates the transition from chronic intestinal inflammation to colon cancer. Nat Commun 2020, 11.
26. Kohler LHF, Reich S, Yusenko M, Klempnauer K-H, Begemann G, Schobert R, Biersack B. Multimodal 4-arylchromene derivatives with microtubule-destabilizing, anti-angiogenic, and MYB-inhibitory activities. Cancer drug Resist (Alhambra Calif). 2023;6:59–77.
27. Chen Y, Zhu S, Chen Z, Liu Y, Pei C, Huang H, Hou S, Ning W, Liang J. Gingerenone A alleviates ferroptosis in secondary liver injury in colitis mice via activating Nrf2-Gpx4 signaling pathway. J Agric Food Chem. 2022;70:12525–34.
28. Liang J, Dai W, Liu C, Wen Y, Chen C, Xu Y, Huang S, Hou S, Li C, Chen Y et al. Gingerenone A attenuates Ulcerative Colitis via Targeting IL-17RA to inhibit inflammation and restore intestinal barrier function. Adv Sci 2024.
29. Chen Y-e, Xu S-j, Lu Y-y, Chen S-x, Du X-h, Hou S-z, Huang H-y, Liang J. Asperuloside suppressing oxidative stress and inflammation in DSS-induced chronic colitis and RAW 264.7 macrophages via Nrf2/HO-1 and NF-κB pathways. Chemico-Biol Interact 2021, 344.
30. Chen Y, Yuan X, Pei C, Deng Z, Du X, Liang J, He L, Hou S. Vitexin alleviates breast tumor in mice via skewing TAMs toward an iNOS < SUP>+ profile orchestrating effective CD8 < SUP>+ T cell activation. J Funct Foods 2022, 95.
31. Dong Y, Zhu G, Wang S-F, Keon KA, Rubinstein JL, Zeng S-X, Zhang S, Chen Q-L, Fu J, Li M, et al. Toosendanin, a novel potent vacuolar-type H plus -translocating ATPase inhibitor, sensitizes cancer cells to chemotherapy by blocking protective autophagy. Int J Biol Sci. 2022;18:2684–702.
32. Yang H, Liu Y, Zhao M-M, Guo Q, Zheng X-K, Liu D, Zeng K-W, Tu P-F. Therapeutic potential of targeting membrane-spanning proteoglycan SDC4 in hepatocellular carcinoma. Cell Death Dis 2021, 12.
33. Luo W, Lin K, Hua JY, Han JB, Zhang QY, Chen LF, Khan ZA, Wu GJ, Wang Y, Liang G. Schisandrin B attenuates diabetic Cardiomyopathy by targeting MyD88 and inhibiting MyD88-dependent inflammation. Adv Sci 2022, 9.
34. Takada I, Makishima M. Control of inflammatory bowel disease and colorectal cancer by synthetic vitamin D receptor ligands. Curr Med Chem. 2017;24:868–75.
35. Chen S, Liu H, Li Z, Tang J, Huang B, Zhi F, Zhao X. Epithelial PBLD attenuates intestinal inflammatory response and improves intestinal barrier function by inhibiting NF-κB signaling. Cell Death Dis 2021, 12.
36. Liang C, Jiang Y, Sun L. Vitexin suppresses the proliferation, angiogenesis and stemness of endometrial cancer through the PI3K/AKT pathway. Pharm Biol. 2023;61:581–9.
37. Najafipour R, Momeni AM, Mirmazloomi Y, Moghbelinejad S. Vitexin induces apoptosis in MCF-7 breast Cancer cells through the regulation of specific miRNAs expression. Int J Mol Cell Med. 2022;11:197–206.
38. Wang Q, Zhang J, Ye J, Guo J. Vitexin exerts anti-tumor and anti-angiogensis effects on cervical cancer through VEGFA/VEGFR2 pathway. Eur J Gynaecol Oncol. 2022;43:86–91.
39. Zhang J, Liang F, Chen Z, Chen Y, Yuan J, Xiong Q, Hou S, Huang S, Liu C, Liang J. Vitexin protects against dextran sodium sulfate-induced colitis in mice and its potential mechanisms. J Agric Food Chem 2022.
40. Vernia F, Valvano M, Longo S, Cesaro N, Viscido A, Latella G. Vitamin D in inflammatory bowel diseases. mechanisms of action and therapeutic implications. Nutrients 2022, 14.
41. Chen J, Ruan X, Yuan S, Deng M, Zhang H, Sun J, Yu L, Satsangi J, Larsson SC, Therdoratou E, et al. Antioxidants, minerals and vitamins in relation to Crohn's disease and ulcerative colitis: a mendelian randomization study. Aliment Pharmacol Ther. 2023;57:399–408.
42. Garcia-Martinez JM, Chocarro-Calvo A, Martinez-Useros J, Regueira-Acebedo N, Fernandez-Acenero MJ, Munoz A, Larriba MJ, Garcia-Jimenez C. SIRT1 mediates the antagonism of Wnt/β-catenin pathway by vitamin D in colon carcinoma cells. *bioRxiv* 2024.
43. Zhang Y, Xie J. Targeting ferroptosis regulators by natural products in colorectal cancer. Front Pharmacol 2024, 15.
44. Xia X, Xu F, Dai D, Xiong A, Sun R, Ling Y, Qiu L, Wang R, Ding Y, Lin M et al. VDR is a potential prognostic biomarker and positively correlated with immune infiltration: a comprehensive pan-cancer analysis with experimental verification. Biosci Rep 2024, 44.
45. Tocchini-Valentini G, Rochel N, Wurtz JM, Moras D. Crystal structures of the vitamin D nuclear receptor liganded with the vitamin D side chain analogues calcipotriol and seocalcitol, receptor agonists of clinical importance. Insights into a structural basis for the switching of calcipotriol to a receptor antagonist by further side chain modification. J Med Chem. 2004;47:1956–61.
46. Sun W, Chen J, Li J, She X, Ma H, Wang S, Liu J, Yuan Y. Vitamin D receptor-deficient keratinocytes-derived exosomal miR-4505 promotes the macrophage polarization towards the M1 phenotype. Peerj 2023, 11.
47. Zhang Y, Zhou J, Hua L, Li P, Wu J, Shang S, Deng F, Luo J, Liao M, Wang N et al. Vitamin D receptor (VDR) on the cell membrane of mouse macrophages participates in the formation of lipopolysaccharide tolerance: mVDR is related to the effect of artesunate to reverse LPS tolerance. Cell Communication Signal 2023, 21.
48. Li D-M, Zhang J, Li W-M, Cui J-T, Pan Y-M, Liu S-Q, Xing R, Lu Y-Y. MAWBP and MAWD inhibit proliferation and invasion in gastric cancer. World J Gastroenterol. 2013;19:2781–92.
49. Li A, Yan Q, Zhao X, Zhong J, Yang H, Feng Z, Du Y, Wang Y, Wang Z, Wang H, et al. Decreased expression of PBLD correlates with poor prognosis and functions as a tumor suppressor in human hepatocellular carcinoma. Oncotarget. 2016;7:524–37.
50. Wu J, Niu Q, Yuan J, Xu X, Cao L. Novel compound cedrelone inhibits hepatocellular carcinoma progression via PBLD and Ras/Rap1. Experimental Therapeutic Med. 2019;18:4209–20.
51. Liang Y, Song X, Li Y, Su P, Han D, Ma T, Guo R, Chen B, Zhao W, Sang Y et al. vol 38, pg 6850, : circKDM4C suppresses tumor progression and attenuates doxorubicin resistance by regulating miR-548p/PBLD axis in breast cancer (2019). *Oncogene* 2021, 40:2816–2816.

Publisher's note